Inorganic Chemistry

Article

pubs.acs.org/IC

Tuning the Photochromic Properties of Molybdenum Bisphosphonate Polyoxometalates

Hani El Moll,[†] Anne Dolbecq,[†] Israël Martyr Mbomekalle,[†] Jérôme Marrot,[†] Philippe Deniard,[‡] Rémi Dessapt,*[,‡] and Pierre Mialane*[,†]

[†]Institut Lavoisier de Versailles, UMR 8180, Université de Versailles Saint-Quentin en Yvelines, 45 Avenue des Etats-Unis, 78035 Versailles cedex, France

[‡]Institut des Matériaux Jean Rouxel, Université de Nantes, CNRS, 2 rue de la Houssinière, BP 32229, 44322 Nantes cedex, France

Supporting Information

ABSTRACT: Seven hybrid organic−inorganic bisphosphonate molybdenum(VI) polyoxometalate complexes with the general formula $[(Mo_3O_8)_4(O_3PC(C_mH_{2m}NRR'R'')(O)PO_3)_4]^{8-}$ (m = 3; R, R′, and R″ = H or CH_3) and $[(Mo_3O_8)_2(O)(O_3PC(C_mH_{2m}NRR'R'')(O)PO_3)_2]^{6-}$ (m = 3 or 4; R, R′, and R″ = H or CH_3) have been synthesized and their structures solved using single-crystal X-ray diffraction. These compounds are made of a $\{Mo_{12}\}$ or a $\{Mo_6\}$ inorganic core functionalized by various alkylammonium bisphosphonates, with these ligands differing by the length of their alkyl chains and the number of methyl groups grafted on the N atom. The nature of the counter-cations (Na^+, K^+, Rb^+, Cs^+, and/or NH_4^+) constituting these materials has also been modulated. ^{31}P NMR spectroscopic studies in aqueous media have shown that all the dodecanuclear complexes reported here are stable in solution, whereas for the hexanuclear compounds, a dynamic equilibrium between two isomers has been evidenced, and the corresponding standard thermodynamic parameters determined for one of them. The electrochemical properties of six representative compounds of this family have been investigated. It has been found that the Mo^{6+}/Mo^{5+} reduction potential is similar for all the polyoxometalates studied. Besides, it is shown that electrochemical cycling is an efficient method for the deposition of these compounds on a surface. The photochromic properties of all the complexes reported herein have been studied in the solid state. Under irradiation in the near ultraviolet (UV), the $\{Mo_{12}\}$ systems shift from white to reddish-brown, while the $\{Mo_6\}$ compounds develop a purple coloration. The coloration kinetics has been systematically quantified and the optical band gaps, the salient coloration kinetic parameters and the coloration kinetic half-life times have been determined. This has evidenced that several of these materials develop very strong and rapid UV-induced color changes, with remarkable coloration contrasts. Finally, the optical properties of these systems are discussed in light of several salient parameters as the POM topology, the nature of the grafted bisphosphonate ligand, and the design of the hydrogen-bonding network at the organic−inorganic interface.

1. INTRODUCTION

Although the first polyoxometalate (POM) compounds with covalently attached organic groups was isolated at the beginning of the 20th century,[1] it is only since 1975 that the interest for the chemistry of hybrid organic−inorganic POMs has exploded.[2] It has thus been demonstrated that the presence of bonded organic ligands at the surface of inorganic polyanions can allow the elaboration of unique materials or devices, as demonstrated by the characterization of surfaces patterned with covalently grafted POMs,[3] polymers with controlled topologies,[4] or extended frameworks based on POM building units.[5] Concomitantly to the characterization of such composite systems, it has been shown that hybrid POMs can exhibit very interesting properties. Especially, catalytic activities[6] or biological properties such as tumor cell killing[7] have been evidenced for various organic−inorganic POMs. Focusing now on the optical properties of hybrid POMs, until recently, only the behavior of ionic systems associating cationic organic molecules and inorganic polyanions have been significantly studied.[8] The nonlinear optical activity of salts combining stilbazolium cations and POMs has thus been evidenced.[9] Besides, the photochromic properties of compounds made of polyanions (mainly polyoxomolybdates) and organic cations (mainly organoammonium cations (OACs)) have been studied.[10] Such materials can develop very strong ultraviolet (UV)-induced color changes, with remarkable coloration contrast. They may be viewed as efficient devices with potential applications such as smart painting, cosmetic, optical power-limiting switches, or UV sensors. Especially, in these fields, challenging developments necessitate the elaboration of new devices that can be miniaturized at will.[11] With this aim, new photochromic hybrid organic−inorganic POM materials, obtained following a bottom-up approach, constitute an attractive answer. In addition, such materials present several advantages for the design of new photochromic devices, such as low density, transparency, and processability. Interestingly, it has been shown that their photochromic properties (photogenerated hue, coloration, and fading speeds) are highly tunable, and are strongly dependent on the nature of both the organic and inorganic components.[10b,c] Indeed, POM materials with efficient photochromic behavior are obtained only when the OACs possess at least one N^+−H group in hydrogen bonding interaction with the POM unit. In order to rationalize these observations, mechanisms

Received: October 26, 2011
Published: January 27, 2012

   dx.doi.org/10.1021/ic202299d | Inorg. Chem. 2012, 51, 2291−2302

associating a cation−anion intermolecular proton transfer and an $O^{2-} \rightarrow Mo^{6+}$ intramolecular charge transfer have been proposed.[10a,b] However, this involves inorganic POM units that are not intrinsically photochromic, with the consequence that a given molecular material which contains suitable POMs and OACs may not develop a photochromic response, because of the lack of direct hydrogen-bonding interactions between both the organic and inorganic components. Another fatal consequence is that such ionic hybrid POM materials can loose their photochromic properties after, for example, their dissolution in polar solvent, or their incorporation in a given matrix (metal-organic framework, zeolite, ...).

Bisphosphonate ligands are known to be efficient for the structuration of POMs.[12] Very recently, we have shown that related hybrid POM systems possessing intrinsic photochromic properties can be prepared.[13] The synthetic strategy consists of grafting directly on the inorganic core of POM bisphosphonate ligands that possess an alkylammonium group. It was thus shown that the dodecanuclear complex $Na_7(N(C_4H_9)_4)[(Mo_3O_8)_4(O_3PC(C_3H_6NH_3)(O)PO_3)_4]\cdot 43H_2O$, which contains four $R-NH_3^+$ arms in interaction with the $\{Mo_{12}\}$ core and does not possess any countercation able to transfer a proton to the inorganic moiety, can shift from white to reddish-brown ($t_{1/2}$ = 8 min) under 365-nm UV irradiation (12 W), and this in the solid state. However, although the chemical and photochemical characterization of $Na_7(N(C_4H_9)_4)[(Mo_3O_8)_4(O_3PC(C_3H_6NH_3)(O)PO_3)_4]\cdot 43H_2O$ allowed validating the adopted approach, it appears obvious that it must be possible to isolate related materials with better photoresponses. This must be reachable either by playing on the nature of the organic arm attached to the POM core or by modulating the topology of the molybdenum cluster. Besides, and importantly, the enlargement of this new class of material could also allow a better understanding of the parameters (topology of the POM cluster, number and strength of the hydrogen bonds, nature of the O atom involved in the H···O interaction, ...) governing the optical properties of hybrid photochromic POM compounds.

Here, we report on the characterization of seven hybrid bisphosphonate molybdenum(VI) POM complexes. These compounds are made of various alkylammonium bisphosphonate ligands (see Scheme 1) grafted on either a $\{Mo_{12}\}$ or a $\{Mo_6\}$ fragment (see Figure 1). The optical properties of all these systems in their ground state and under UV irradiation are reported. Their photochromic properties have been investigated using diffuse reflectance spectroscopy, and the kinetics of coloration are discussed in light of their structural characteristics. The electrochemical properties of selected compounds have been studied. Finally, nuclear magnetic resonance (NMR) studies have been performed in order to determine the stability of these materials in solution, which is a very important feature for further use of these systems (deposition on surfaces, insertion in matrices).

Scheme 1. Representation of the Bisphosphonate Ligands (Protonated Form) Used in This Study

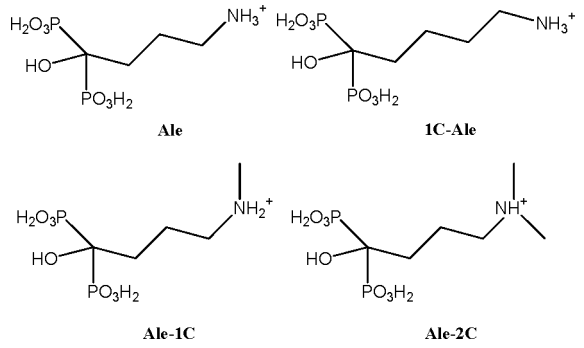

2. RESULTS AND DISCUSSION

2.1. Synthesis and Structural Description of the Compounds. All the crystallographic data of the seven reported compounds are gathered in Table 1, and their structures are represented in Figure 1. They all contain a Mo(VI) dodecanuclear (noted $\{Mo_{12}\}$) or hexanuclear (noted $\{Mo_6\}$) core with grafted functionalized bisphosphonate ligands (see Scheme 1). The $\{Mo_{12}\}$ compounds are synthesized in moderate yield (12−30%) and the $\{Mo_6\}$ ones in good yield (40−56%). These systems have been obtained either at room temperature or under hydrothermal conditions (130 °C). The nature of the Mo precursor plays an important role on the nuclearity of the POM cluster. Obviously, the $\{Mo_{12}\}$ systems can be obtained only in the presence of Na cations, thus starting from $Na_2MoO_4\cdot 2H_2O$, while $(NH_4)_6Mo_7O_{24}\cdot 4H_2O$ is used as the Mo source for the synthesis of the $\{Mo_6\}$ species. However, the role of the pH is also crucial. Indeed, the $\{Mo_{12}\}$ family is obtained at pH 3, while the $\{Mo_6\}$ compounds are synthesized at pH 4.7, a pH at which it has not be possible to obtain $\{Mo_{12}\}$ systems, even in the presence of alkaline ions.

The topology of the $\{Mo_{12}\}$ unit in **Mo_{12}−Ale−1C** and **Mo_{12}−Ale−2C** is similar to that found recently in the compound $Na_2Rb_6[(Mo_3O_8)_4(O_3PC(R)(O)PO_3)_4]\cdot 43H_2O$ (R = $C_3H_6NH_3$) (**Mo_{12}−Ale**).[7] In these materials, the $\{Mo_{12}\}$ block is built upon the assembly of four equivalent trimeric subunits around a central Na atom, which acts as an assembling group (Figure 1a), explaining the crucial role of this alkaline ion in the synthetic process. Each trimeric unit is composed of a $\{Mo_2O_9\}$ dimer, formed by two faced-shared $\{MoO_6\}$ octahedra, corner-shared connected with a third monomeric $\{MoO_6\}$ octahedron. A bisphosphonate ligand is covalently grafted into each trimeric subunit and links the three Mo^{6+} cations. The $\{Mo_{12}\}$ cores only differ by the number of methyl substituents on the amino group, which is 0 in **Mo_{12}−Ale**, 1 in **Mo_{12}−Ale−1C** and 2 in **Mo_{12}−Ale−2C** (Scheme 1 and Figure 1a). This drastically impacts the hydrogen-bonding network established between the ammonium functions and the $\{Mo_{12}\}$ cores. Importantly, while **Mo_{12}−Ale** develops intramolecular and intermolecular hydrogen bonds, **Mo_{12}−Ale−1C** develops only intramolecular hydrogen bonds and in **Mo_{12}−Ale−2C**, only intermolecular hydrogen bounds are found (see Table SI1 in the Supporting Information). This highlights that small variations of the organic part of the hybrid POM can have drastic influences on the hydrogen-bonding network.

Mo_6−Ale, **Mo_6−Ale−1C_a**, **Mo_6−Ale−1C_b**, **Mo_6−Ale−2C**, and **Mo_6−1C−Ale** are all made of the $\{Mo_6\}$ complex, which has the general formula $[(Mo_3O_8)_2(O)(O_3PC(R)(O)PO_3)_2]^{6-}$. This block is built upon two corner-shared trimeric units, similar to those found in the $\{Mo_{12}\}$ clusters described above. However, the $\{Mo_6\}$ core presents two conformations in the solid state (hereafter labeled A and B conformations). The A conformation (Figure 1b), which has been previously observed by Sergienko et al.,[14] has the approximate C_{2h} symmetry. The six Mo^{6+} cations are localized in the same plane, and the oxygen atom common to the two trimeric units is positioned on a pseudo-inversion center. At the opposite, the B conformation

dx.doi.org/10.1021/ic202299d | Inorg. Chem. 2012, 51, 2291−2302

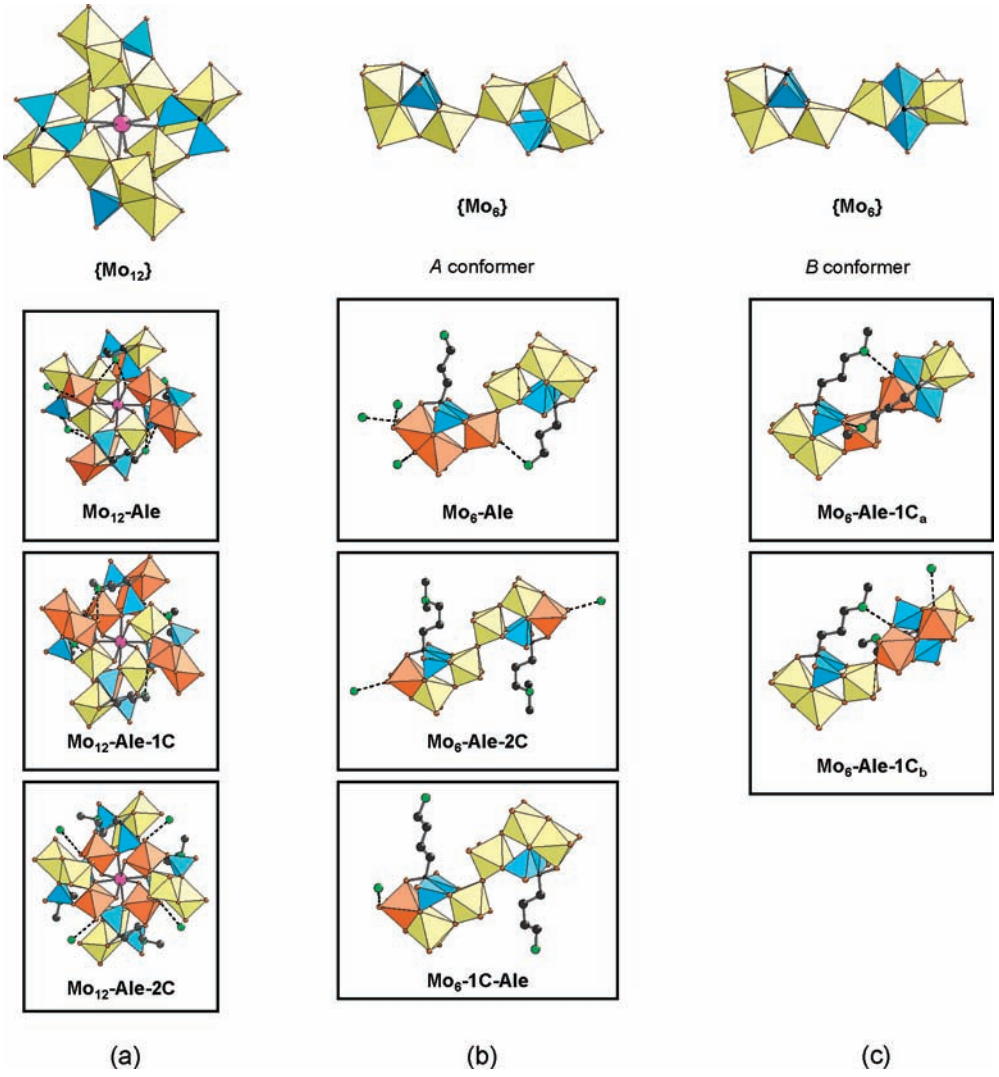

Figure 1. Representation of (a) the $\{Mo_{12}\}$-based polyanions **Mo_{12}–Ale**, **Mo_{12}–Ale–1C**, and **Mo_{12}–Ale–2C**; (b) the $\{Mo_6\}$-based (*A* conformers) polyanions **Mo_6–Ale**, **Mo_6–Ale–2C**, and **Mo_6–1C–Ale**; (c) the $\{Mo_6\}$-based (*B* conformers) polyanions **Mo_6–Ale–1C_a** and **Mo_6–Ale–1C_b**. The H atoms are omitted for clarity. The intramolecular and intermolecular hydrogen bonds between the $\{-NH_{3-x}Me_x\}^+$ head of the bisphosphonate ligands and the O atoms of the inorganic core are represented as dotted lines. Only the N atom of the POMs involved in the intermolecular hydrogen bonds are represented. The $\{MoO_6\}$ octahedra involved in hydrogen-bonding interaction are depicted in orange color.

(Figure 1c) has the approximate C_1 symmetry, and the two trimeric units are twisted in two perpendicular planes. The A conformation is observed in **Mo_6–Ale**, **Mo_6–Ale–2C**, and **Mo_6–1C–Ale** (Figure 1b), while **Mo_6–Ale–1C_a** and **Mo_6–Ale–1C_b** contain the B conformation (Figure 1c). This configuration has also been recently evidenced by Wang et al.[15] The existence of the A and B $\{Mo_6\}$ conformers can be justified considering that the two trimeric units constituting these species can easily rotate around their common O atom. Obviously, such phenomenon cannot be observed for the $\{Mo_{12}\}$ species. It has not been possible to clearly discriminate the parameters favoring the crystallization of a given $\{Mo_6\}$ conformer. Moreover, NMR solution studies indicate that the A and B species are close in energy (see below). Let us notice that **Mo_6–Ale–1C_a** and **Mo_6–Ale–1C_b** are diverging only by the nature of the counterions (rubidium and ammonium for **Mo_6–Ale–1C_a** and cesium, potassium, and ammonium for **Mo_6–Ale–1C_b**). In **Mo_6–1C–Ale**, the bisphosphonate ligand contains an additional $\{CH_2\}$ group in the alkyl chain, compared to the alendronate ligand (see Scheme 1). Finally, as in the case of the $\{Mo_{12}\}$ systems, the variation of the nature of the bisphosphonate ligand has allowed modulation of the hydrogen-bonding network involving the alkylammonium groups and the inorganic core (see Table SI1 in the Supporting Information), and then potentially their photochromic properties (see below).

2.2. ^{31}P NMR Spectroscopic Characterization. The phosphorus NMR spectrum in water of **Mo_{12}–Ale–1C** presents a doublet of doublet located at 24.71 and 19.68 ppm (^2J = 40.6 Hz), within the range of the molybdenum bisphosphonates previously reported[12] and in agreement with the asymmetric coordination mode of the alendronate ligand adopted in the $\{Mo_{12}\}$ core.[13] A similar ^{31}P NMR signature is observed for **Mo_{12}–Ale–2C**, thus showing that the $\{Mo_{12}\}$ complex is stable in solution. In contrast, the ^{31}P NMR spectrum of **Mo_6–Ale** presents two singlets at 21.63 and 21.36 ppm, with relative intensities of 1.8:0.2 at room temperature. Considering that, in the A conformer observed in **Mo_6–Ale**, the four P atoms are in analogous environments, the two singlets observed in the NMR spectrum are consistent with the

dx.doi.org/10.1021/ic202299d | *Inorg. Chem.* 2012, 51, 2291–2302

Table 1. X-ray Crystallographic Data Related to the Compounds Reported Therein

	Mo_{12}–Ale–1C	Mo_{12}–Ale–2C	Mo_6–Ale	Mo_6–Ale–1C_a	Mo_6–Ale–1C_b	Mo_6–Ale–2C	Mo_6–1C–Ale
formula	$C_{20}H_{90}Mo_{12}N_4Na_2O_{83}P_8Rb_6$	$C_{24}H_{128}Mo_{12}N_4Na_4O_{98}P_8K_4$	$Mo_6P_4C_8H_{61.25}N_{7.75}O_{41}Rb_{0.25}$	$C_{10}H_{69.25}Mo_6N_{7.75}O_{43}P_4Rb_{0.25}$	$C_{10}H_{58}Mo_6N_{6.5}O_{40}P_4Cs_{1.25}K_{0.25}$	$C_{12}H_{56}K_2Mo_6N_6O_{38}P_4$	$C_{10}H_{66}Mo_6N_8O_{41}P_4$
Fw [g]	3672.8	3688.7	1626.1	1707.3	1785.0	1670.3	1654.2
crystal system	triclinic	tetragonal	trigonal	orthorhombic	orthorhombic	monoclinic	monoclinic
space group	$P\bar{1}$	$I4_1/a$	$P\bar{3}$	$Pbca$	$Pbca$	$P2_1/n$	$P2_1$
Z	2	4	6	8	8	2	2
T [K]	293	293	293	293	293	293	293
a [Å]	16.0671(16)	21.739(5)	28.5021(13)	18.409(14)	18.8861(4)	9.6898(6)	14.969(2)
b [Å]	16.3128(16)	21.739(5)	28.5021(13)	16.856(13)	17.0627(4)	18.0280(12)	9.0746(12)
c [Å]	20.8626(19)	26.188(6)	10.5126(10)	36.26(3)	31.6438(7)	14.3741(10)	19.820(3)
α [°]	72.919(2)	90	90	90	90	90	90
β [°]	72.729(2)	90	90	90	90	106.8100(10)	107.679(2)
γ [°]	80.883(2)	90	120	90	90	90	90
V [Å^3]	4976.0(8)	12376(5)	7396.0(9)	11252(14)	10197.1(4)	2403.7(3)	2565.0(6)
ρ_{calc} [g cm^{-3}]	2.171	1.581	2.055	2.000	2.328	2.233	2.121
μ [mm^{-1}]	4.118	1.391	1.960	2.16	2.624	1.933	1.666
reflections collected	24855	33314	57888	47041	136489	18111	19318
unique reflections (R_{int})	15551 (0.103)	5438 (0.101)	14623 (0.105)	8776 (0.176)	14871(0.0525)	6951 (0.096)	13174 (0.066)
refined parameters	973	1029	568	630	657	325	634
$R(F_o)$[a]	0.063	0.057	0.077	0.091	0.0668	0.041	0.039
$R_w(F_o^2)$[b]	0.172	0.169	0.219	0.278	0.0803	0.106	0.097

dx.doi.org/10.1021/ic202299d | Inorg. Chem. 2012, 51, 2291–2302

presence of two species in solution. Besides, the absence of ^2J couplings indicates that, for both species, the P atoms within a ligand are equivalent. We can also note that no resonance can be attributed to free bisphosphonate ligands. A similar behavior is observed for all four of the other reported {Mo_6} compounds.

The presence of two species each characterized by a singlet with very close chemical shifts could be explained, considering that after dissolution of a {Mo_6} compound with a given conformation in the solid state, an equilibrium between the two A and B conformers (see Figures 1b and 1c) occurs in solution. Such equilibrium is made possible due to the easy rotation around the central O atom (see above). Unfortunately, at this stage, it is not possible to unambiguously attribute the NMR peaks, because no clear correlation between the solid-state structures of the {Mo_6} core containing materials and the relative intensity and chemical shifts of the two peaks can be established. However, in order to investigate the equilibrium involving the A and B isomers, the ^{31}P NMR spectrum in D_2O of **Mo_6–Ale–1C$_a$** were recorded at different temperatures in the 275–350 K range. Selected spectra are represented in Figure 2. The two resonances are relatively sharp at low

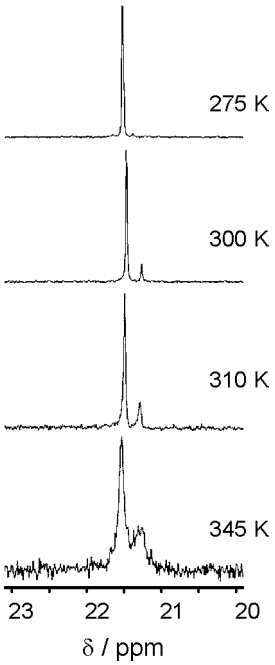

Figure 2. Variable-temperature 300 MHz ^{31}P NMR spectra of complex **Mo_6–Ale–1C$_a$**.

temperature and broaden when the temperature increases, indicating that, as expected, dynamic exchange between the A and B conformers become faster under heating. It appears also that when the temperature increases, the intensity of the main peak decreases. From the integrated signal of the two conformers, the following standard thermodynamic parameters are derived: $|\Delta_R H^0| = 22.9$ kJ mol^{-1} and $|\Delta_R S^0| = 60.8$ J K^{-1} mol^{-1} (see Figure SI1 in the Supporting Information). Finally, the spectrum of a sample heated at 350 K and cooled to room temperature was recorded at 295 K. This one is strictly identical to the spectrum recorded at the same temperature on a freshly dissolved compound, indicating that (i) the equilibrium is reached just after the dissolution of **Mo_6–Ale–1C$_a$**, even at room temperature, and (ii) the {Mo_6} complex is stable over the entire temperature range considered in this study.

2.3. Electrochemical Studies. This section summarizes the electrochemical behavior of six representative compounds, namely **Mo_6–Ale**, **Mo_{12}–Ale**, **Mo_6–Ale–1C**, **Mo_{12}–Ale–1C**, **Mo_6–Ale–2C**, and **Mo_{12}–Ale–2C**. A direct comparison will be done between complexes containing the same organic group (Ale, Ale–1C, or Ale–2C) but different POM blocks ({Mo_6} or {Mo_{12}} cores). This will then be used to highlight the potential influence of the POM topology and the nature of the {$-R-NH_{3-x}Me_x$}$^+$ group on the electrochemical behavior.

The first comparison is between **Mo_6–Ale** and **Mo_{12}–Ale**. Figure 3 presents sets of 10 successive CVs of **Mo_6–Ale** and

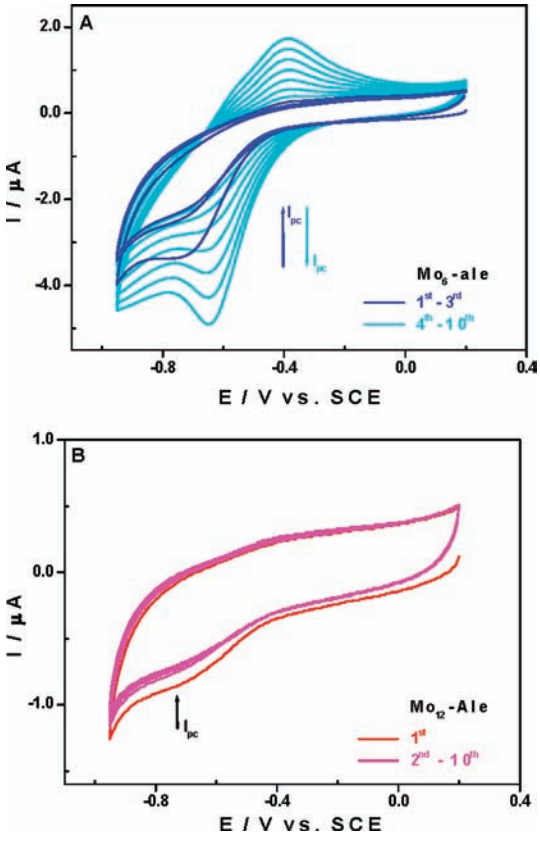

Figure 3. Cyclic voltammograms of **Mo_6–Ale** (A) and **Mo_{12}–Ale** (B) in 0.5 M Li_2SO_4 + H_2SO_4, pH 3. Working electrode, glassy carbon; reference electrode, SCE; scan rate, 50 mV s^{-1}; polyoxometalate concentration, 0.2 mM. Voltage cycling (10 successive scans) is done between +0.2 V and −0.95 V.

Mo_{12}–Ale recorded under the same conditions (see the caption for Figure 3). After a short period of equilibration (first CV to third CV), the reduction current (I_{pc}) grows rapidly and linearly over successive scans for **Mo_6–Ale**, while for **Mo_{12}–Ale**, I_{pc} remains almost constant (see Figure SI2A in the Supporting Information). If we continue the voltage cycling by performing successive sets of 10 CVs (see Figure SI3 in the Supporting Information), we observe that I_{pc} stops increasing after the fourth set for **Mo_6–Ale**, but for **Mo_{12}–Ale**, the increase continues until the 10th set. Although, over successive scans, the evolution of the CV pattern looks quite different, the overall behavior is quite similar for both compounds. For **Mo_{12}–Ale**, the reduction potential value remains constant ($E_{pc} \approx -0.65$ V vs SCE, see Table 2) during the 10 × 10 cycles

dx.doi.org/10.1021/ic202299d | Inorg. Chem. 2012, 51, 2291–2302

Table 2. Reduction Potentials of Compounds Mo_6–Ale, Mo_{12}–Ale, Mo_6–Ale-1C, Mo_{12}–Ale-1C, Mo_6–Ale-2C, and Mo_{12}–Ale-2C

compound	Mo_6–Ale	Mo_{12}–Ale	Mo_6–Ale–1C	Mo_{12}–Ale–1C	Mo_6–Ale–2C	Mo_{12}–Ale–2C
E_{pc} (V vs SCE)	−0.65	−0.65	−0.61	−0.57, −0.81	−0.65	−0.65

while I_{pc} grows continuously (see Figure SI2B in the Supporting Information). These observations suggest that there is a slow and gradual formation of a deposit on the working electrode surface. In contrast, for **Mo_6–Ale**, while I_{pc} grows rapidly and reaches saturation very quickly, a slight decrease of the reduction potential value is observed (from −0.65 V to −0.75 V vs SCE). This phenomenon is commonly observed when the film that forms on the working electrode surface becomes thicker and thicker. Under these conditions, the least-negative value observed for E_{pc} will be the one closest to its real value. Therefore, cycling seems to be an easy and efficient method for the deposition of these compounds on the working electrode surface, without decomposition of the starting materials. A scanning electron microscopy (SEM) image of the **Mo_6–Ale** functionalized electrode (see Figure SI4 in the Supporting Information) together with energy-dispersive X-ray (EDX) analysis, which confirm the presence of elemental Mo and P, reveal the homogeneity of the deposited film. Besides, cycling also has the advantage of increasing the electrochemical signal (the reduction current in this case), making comparisons easier.

Mo_6–Ale–1C shows a behavior (see Figure SI5 in the Supporting Information) identical to that of **Mo_6–Ale**, i.e., rapid growth of I_{pc} and slight shift of E_{pc} in the direction of negative potentials (see Figure SI3A in the Supporting Information). In contrast, **Mo_{12}–Ale–1C** shows a singular behavior. In the CV of this compound (see Figure 4), two reduction waves appear

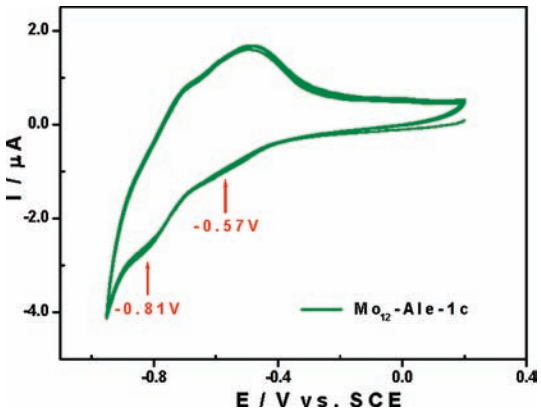

Figure 4. Cyclic voltammograms of **Mo_{12}–Ale–1C** in 0.5 M Li_2SO_4 + H_2SO_4, pH 3. Working electrode, glassy carbon; reference electrode, SCE; scan rate, 50 mV s^{-1}; polyoxometalate concentration, 0.2 mM. Voltage cycling (10 successive scans) is done between +0.2 V and −0.95 V.

distinctly at −0.57 V and −0.81 V vs SCE. In addition, contrary to what we observed with all other compounds, the reduction current (I_{pc}) remains perfectly constant during successive scans. We conclude that the film formed on the working electrode surface quickly stabilizes and does not grow indefinitely. Focusing now on the **Mo_6–Ale–2C** and **Mo_{12}–Ale–2C**, the electrochemical behavior of both these compounds seems identical in all respects. Reduction potentials determined as defined above have exactly the same value for both compounds (E_{pc} = −0.65 V vs SCE) and the reduction current I_{pc} grows similarly (see Figure SI6 in the Supporting Information).

In summary, the electrochemical behavior of these compounds depends on the grafted bisphosphonate ligand (**Ale**, **Ale–1C**, or **Ale–2C**), and can be very different for the {Mo_6} or {Mo_{12}} species as observed for **Mo_6–Ale–1C** and **Mo_{12}–Ale–1C**, or identical as seen with **Mo_6–Ale–2C** and **Mo_{12}–Ale–2C**. In all cases, the reduction potential values are very similar (−0.65 V), only **Mo_{12}–Ale–1C** stands out with a somewhat less-negative reduction potential (−0.57 V).

2.4. Optical Properties. All the powdered materials show a white coloration in their ground state. The optical band gap is ∼375 nm (3.31 eV) for the {Mo_{12}} containing materials and is shifted at higher energy at ∼360 nm (3.45 eV) for compounds which contain the {Mo_6} unit (see Table 3). Under 12 W UV excitation at 365 nm (3.4 eV), the materials show strong photochromic responses with high coloration contrasts, and, as expected,[16] the photoinduced color varies with the nature of the POM. The color of **Mo_{12}–Ale**, **Mo_{12}–Ale–1C**, and **Mo_{12}–Ale–2C** gradually shifts from white to reddish-brown with irradiation time, and, as illustrated in Figure 5a, the color change in **Mo_{12}–Ale–1C** is associated with the growth of a broad absorption band peaking at λ_{max} = 464 nm (2.67 eV), and a second very less-intense absorption band rises up at ∼750 nm (1.65 eV). Let us notice that the optical band gap of **Mo_{12}–Ale**, **Mo_{12}–Ale–1C**, and **Mo_{12}–Ale–2C**, as well as their photoinduced color, perfectly match with those recently reported for the dodecanuclear $Na_6(N(C_2H_5)_2H_2)_2[(Mo_3O_8)_4(O_3PC(C_3H_6NH_3)(O)PO_3)_4]\cdot 25H_2O$ and $Na_7(N(C_4H_9)_4)[(Mo_3O_8)_4(O_3PC(C_3H_6NH_3)(O)PO_3)_4]\cdot 43H_2O$ POMs.[13] Under similar 365 nm UV excitation, **Mo_6–Ale**, **Mo_6–Ale–$1C_a$**, **Mo_6–Ale–$1C_b$**, **Mo_6–Ale–2C**, and **Mo_6–1C–Ale** develop a purple coloration, which becomes darker and darker up when the irradiation time is increased (Figure 5b). By comparison with the results described above, the purple color of the {Mo_6}-containing materials is due to a red shift of the photogenerated absorption band, which is located at λ_{max} = 508 nm (2.44 eV). Let us notice that the optical band gap, as well as the photoinduced purple color, is similar for the materials that contain the {Mo_6} block with A or B conformation.

According to the photochromism mechanism of such hybrid materials, the UV excitation transfers an electron from an O atom of the POM block to the adjacent Mo^{6+} site.[10] This electron/hole pair segregation is coupled with the transfer of a labile hydrogen atom of the ammonium group onto an adjacent {MoO_6} octahedron. The H atom moves along the hydrogen bond and acts as a bolt, which traps the electron on the Mo center by creating a {$Mo^{5+}(OH)O_5$} site. The coloration is then due to the photoreduction of Mo^{6+} ($4d^0$) to Mo^{5+} ($4d^1$) cations and occurs via d–d transitions if the electron injected in the conduction band is trapped onto a specific Mo center, or Mo^{6+}/Mo^{5+} intervalence transfers if it can be delocalized onto several adjacent {MoO_6} octahedra. At this stage, the direct

dx.doi.org/10.1021/ic202299d | Inorg. Chem. 2012, 51, 2291–2302

Table 3. Optical Characteristics and Coloration Kinetic Parameters of the Compounds Reported Therein

	Mo_{12}–Ale	Mo_{12}–Ale-1C	Mo_{12}–Ale-2C	Mo_6–Ale	Mo_6–Ale–1C_a	Mo_6–Ale–1C_b	Mo_6–Ale–2C	Mo_6–1C–Ale
E_g (eV)[a]	3.31	3.32	3.31	3.45	3.44	3.46	3.43	3.45
λ_{max} (nm)[b]	464	464	464	508	508	508	508	508
$R^i(0)$[c]	0.888	0.843	0.831	0.892	0.916	0.954	0.908	0.931
a[d]	0.842	0.766	0.613	0.799	0.704	0.837	0.774	0.787
b[d]	0.122	0.184	0.019	0.348	0.032	0.209	0.078	0.175
R^2[e]	0.999	0.996	0.999	0.997	0.999	0.993	0.999	0.995
$t_{1/2}$ (min)[f]	8.20	5.44	51.81	2.87	31.25	4.78	12.82	5.71

[a]Optical band gap (eV). [b]Photoinduced absorption band wavelength. [c]Reflectivity value before UV excitation (t = 0) at irradiation i = 464 nm for the {Mo_{12}} compounds and i = 508 nm for the {Mo_6} compounds. [d]Salient coloration kinetic parameters. [e]Regression coefficient for the $R(t)$ vs t plots. [f]Coloration kinetic half-life time (min).

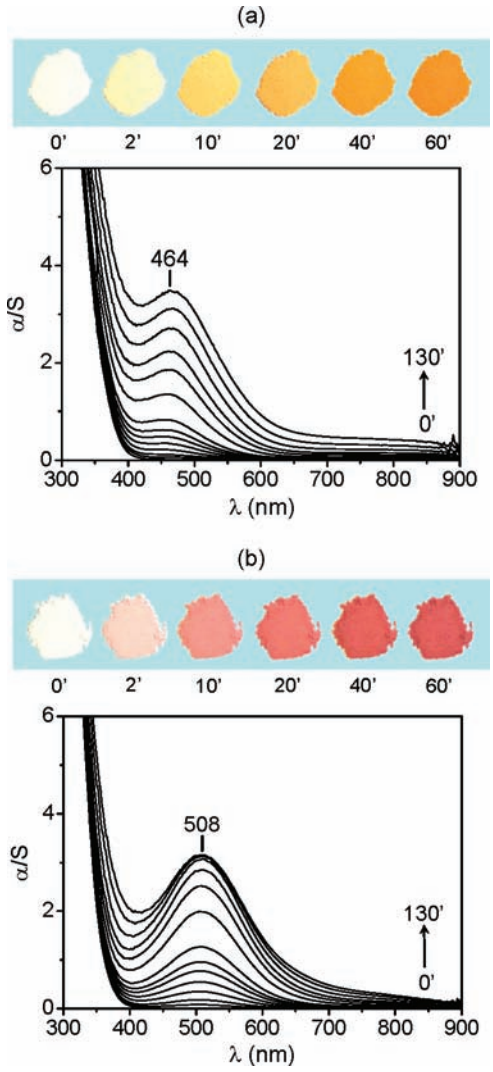

Figure 5. Kubelka–Munk transformed reflectivity of (a) **Mo_{12}–Ale–1C** and (b) **Mo_6–Ale** measured in the 300–900 nm after 0, 1, 2, 4, 6, 8, 10, 12.5, 20, 30, 40, 60, 90, and 130 min of 365 nm UV irradiation. Color of **Mo_{12}–Ale–1C** and **Mo_6–Ale** after 0, 2, 5, 10, 20, 40, and 60 min UV irradiation at 365 nm.

correlation between the topology of the {Mo_6} and {Mo_{12}} units and the position in energy of their photogenerated absorption bands involve precisely identifying the localization of the Mo^{5+} centers, which, unfortunately, is a hard task to achieve, because d–d transitions and intervalence transfers can not be easily discriminated. However, in an empirical way, we have observed that, in photochromic hybrid POM systems, the absorption bands in the excited state are generally red-shifted as the corner-shared connection between the {MoO_6} octahedra increases, which should favor the electronic delocalization via intervalence transfers. This often arises when increasing the size as well as the dimensionality of the POM.[10b,c] Both the {Mo_{12}} and {Mo_6} complexes are built upon the same {Mo_3} subunit, but in the {Mo_{12}} core, the four {Mo_3} blocks are connected together via P–O–Mo bonds and not via direct Mo–O–Mo bonds. So, at first sight, the electrons could be only localized inside the {Mo_3} entities and the absorption band is located at 464 nm. On the other hand, the two {Mo_3} subunits of the {Mo_6} core are directly connected via corner sharing, that extends the connection between the {MoO_6} octahedra, and the {Mo_6} complexes develop a red-shifted absorption band peaking at 508 nm.

Concomitant to the reduction of the POM unit, the hole is transferred on the N atom of the organic component, which creates a spatial segregation of the electron on the mineral part and the hole on the organic one. This banishes the fast electron/hole recombination in the POM and allows one to maintain the coloration when the UV irradiation is switched off. The excited state—and, therefore, the coloration—is stable under ambient conditions for a certain time, depending on the UV irradiation duration, and then the back oxidation of the photoreduced Mo^{5+} cations by O_2 induces the bleaching of the materials (typically, for an irradiation duration of 25 min, which corresponds to ∼90% of the photoreduced Mo^{5+} cations (see the Supporting Information), the purple color of **Mo_6–Ale** totally disappears after 10 h). The bleaching process of all the studied materials is strongly accelerated by keeping the samples under moderate heating at 40 °C (in this condition, the purple coloration of **Mo_6–Ale** disappears after a few minutes). To date, ∼20 coloration/fading cycles under ambient conditions, as well as at 40 °C, can be performed without detecting any fatigue resistance with the naked eye.

The coloration kinetics, under ambient conditions, of the seven compounds reported here, together with that of **Mo_{12}–Ale**, has been systematically quantified by analyzing the evolution of the diffuse reflectivity spectra as a function of the UV irradiation time. As we recently demonstrated,[10b,c,13] in photochromic hybrid POM materials, the decrease of $R^{\lambda max}(t)$ (i.e., the reflectivity at the maximum wavelength of the absorption) with the irradiation time is correlated to the decrease of the concentration of reducible Mo^{6+} cations, which occurs according to a pseudo-second-order kinetic law (see the Supporting Information for the detailed coloration kinetic model). The $R^{\lambda max}(t)$ vs t curve, relative to the seven materials, can be perfectly fitted as $R^{\lambda max}(t) = a/(bt + 1) + R^{\lambda max}(\infty)$ (see Figure SI7 in the Supporting Information). $R^{\lambda max}(\infty)$ is the reflectivity value at the

dx.doi.org/10.1021/ic202299d | Inorg. Chem. 2012, 51, 2291–2302

end of the photochromic process, that is, at $t = \infty$. The a parameter is defined as

$$a = R^{\lambda_{max}}(0) - R^{\lambda_{max}}(\infty)$$

i.e., the difference between the reflectivity values just before UV illumination ($t = 0$) and at $t = \infty$. The b parameter is defined as

$$b = k_c \times C_{6+,r}(0)$$

where k_c is the coloration rate constant, and $C_{6+,r}(0)$ is the initial concentration of photoreducible Mo^{6+} centers per unit volume. In a series of materials built upon the same POM unit (then which develop the same photogenerated absorption bands), the relative coloration rate constants k_i/k_j of two materials i and j can be extracted from the ratio of the slopes of the linear $[R^{\lambda_{max}}(t) - R^{\lambda_{max}}(\infty)]^{-1}$ vs t plots, to compare their coloration speeds (see Table SI3 in the Supporting Information). Table 3 summarizes the kinetic parameters related to the color change of the reported materials.

The coloration kinetics studies of the $\{Mo_{12}\}$ and the $\{Mo_6\}$ series are discussed separately below. In a first part, the coloration kinetics of **Mo_{12}–Ale** has been compared to that of $Na_6(N(C_2H_5)_2H_2)_2[(Mo_3O_8)_4(O_3PC(C_3H_6NH_3)(O)PO_3)_4]\cdot 25H_2O$,[13] which contains the same $\{Mo_{12}\}$ core with very similar hydrogen-bonding interactions between the $\{NH_3^+\}$ groups of the alendronate ligands and the $\{MoO_6\}$ octahedra. The linear $[R^{464}(t) - R^{464}(\infty)]^{-1}$ vs t plots are displayed in Figure 6a (details of the kinetics parameters related to $Na_6(N(C_2H_5)_2H_2)_2[(Mo_3O_8)_4(O_3PC(C_3H_6NH_3)(O)PO_3)_4]\cdot 25H_2O$ are given in the Supporting Information). As expected, both materials show a quite similar coloration speed, with a relative coloration rate constant of 1.01, and a $t_{1/2}$ value of ~8.2 min. This clearly confirms our assumption that, for materials that contain the same $[(Mo_3O_8)_4(O_3PC(R)(O)PO_3)_4]^{8-}$ anion with a quasi-similar hydrogen bonding network, the intrinsic photochromic process is not influenced by the packing with the other countercations. In a second part, the coloration kinetics of **Mo_{12}–Ale–1C** and **Mo_{12}–Ale–2C** have been compared to that of **Mo_{12}–Ale** (Figure 6b). The relative coloration rate constants are 1.68 and 0.21 for **Mo_{12}–Ale–1C** and **Mo_{12}–Ale–2C**, respectively. Hence, the coloration speed varies with the nature of the $\{Mo_{12}\}$ block, and it increases in the order **Mo_{12}–Ale–2C** ≪ **Mo_{12}–Ale** < **Mo_{12}–Ale–1C**, with $t_{1/2}$ values of 51.81, 8.20, and 5.44 min, respectively.

Figure 6c displays a comparison between the $[R^{508}(t) - R^{508}(\infty)]^{-1}$ vs t plots for compounds **Mo_6–Ale**, **Mo_6–Ale–$1C_a$**, **Mo_6–Ale–$1C_b$**, **Mo_6–Ale–2C**, and **Mo_6–1C–Ale**. In this series, the coloration speed increases in the order **Mo_6–Ale–$1C_a$** ≪ **Mo_6–Ale–2C** ≪ **Mo_6–1C–Ale** ≈ **Mo_6–Ale–$1C_b$** < **Mo_6–Ale** with $t_{1/2}$ of 31.25, 12.82, 5.71, 4.78, and 2.87 min, respectively. These kinetics studies highlight the fact that the photochromic properties of polyanions functionalized by bisphosphonate ligands are highly tunable, and a wide range of coloration speed is accessible notably by modifying the design of the grafted alendronate ligands. Among seven materials, **Mo_6–Ale** has the fastest coloration speed, and, to date, this material is one of the most-efficient reported photochromic hybrid POMs. Three major parameters which should influence the coloration speeds of the studied materials are listed below:

(1) *The redox properties of the POM.* According to the photochromism mechanism described above, the UV excitation induces $O^{2-} \rightarrow Mo^{6+}$ intramolecular charge transfer and the photoreduction of Mo^{6+} cations into Mo^{5+} ones. Therefore, the coloration speed should be dependent on the redox properties of the $\{Mo_{12}\}$ and $\{Mo_6\}$ units, considering that the easier the reduction of the POM, the faster the coloration speed.

(2) *The nature of the functionalized alendronate ligands.* As the photochromism mechanism induces the displacement of a H atom from the OAC onto the POM unit, the coloration kinetics is strongly correlated to the strength of the N^+–H bonds, considering that, at first sight, the lower the energy of the N^+–H bond, the faster the coloration speed.[10b] In the reported compounds, the variations on the bisphosphonate ligands grafted on the $\{Mo_{12}\}$ or $\{Mo_6\}$ cores (alkyl side-chain length, methylation degree of the amino group) should affect the strength of the N^+–H bonds.

(3) *The number and the positioning of the hydrogen bonds directly established between both the organic and inorganic components.* The design of the hydrogen-bonding network at the organic–inorganic interface—i.e., the surface

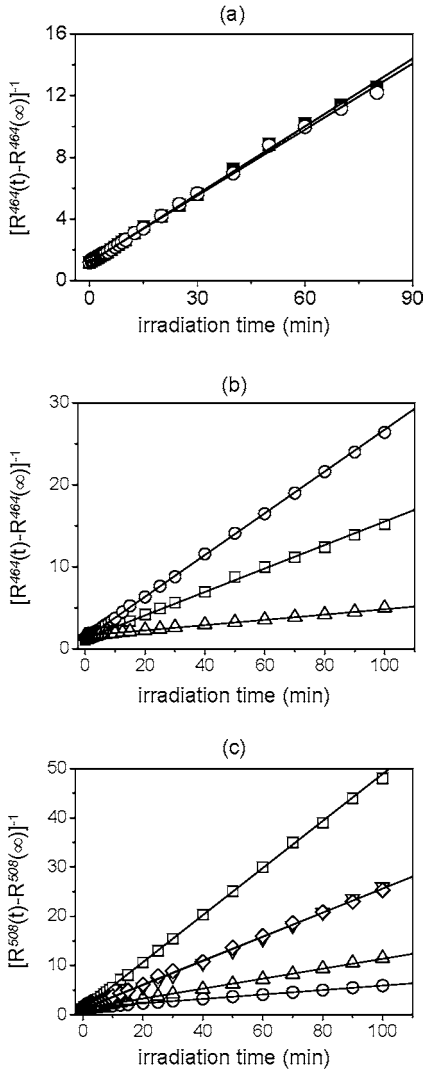

Figure 6. (a) Linear $[R^{464}(t) - R^{464}(\infty)]^{-1}$ vs t plots for (○) **Mo_{12}–Ale** and (■) $Na_6(N(C_2H_5)_2H_2)_2[(Mo_3O_8)_4(O_3PC(C_3H_6NH_3)(O)PO_3)_4]\cdot 25H_2O$. (b) Linear $[R^{464}(t) - R^{464}(\infty)]^{-1}$ vs t plots for (□) **Mo_{12}–Ale**, (○) **Mo_{12}–Ale–1C**, and (△) **Mo_{12}–Ale–2C**. (c) Linear $[R^{508}(t) - R^{508}(\infty)]^{-1}$ vs t plots for (□) **Mo_6–Ale**, (○) **Mo_6–Ale–$1C_a$**, (◇) **Mo_6–Ale–$1C_b$**, (△) **Mo_6–Ale–2C**, and (▽) **Mo_6–1C–Ale**.

dx.doi.org/10.1021/ic202299d | Inorg. Chem. 2012, 51, 2291–2302

where the alkylammonium head of the bisphosphonate organic ligand and the inorganic core interact—is unambiguously another major parameter to take into account to compare the coloration kinetics of the considered compounds.

The identification of the influence of a given parameter, independent of the others, on the coloration speed of the seven materials is a hard task to achieve. However, several pertinent trends can be extracted from the coloration kinetics studies of the $\{Mo_{12}\}$ and $\{Mo_6\}$ series.

First, we can mention that this study confirms that the number and the nature of the hydrogen bonds characterizing each material strongly impact the coloration speeds. **Mo_6−Ale** and **Mo_{12}−Ale−1C**—the best-performing materials of the $\{Mo_6\}$ and $\{Mo_{12}\}$ series—possess a great number of hydrogen bonds in the range of 2.8−3.2 Å (1.75 and 2 per $\{Mo_3\}$ subunit, respectively), and the N−H···O interactions involve several $\{MoO_6\}$ octahedra (3 for **Mo_6−Ale** and 8 for **Mo_{12}−Ale−1C**) (see Figure 1 and Table SI1 in the Supporting Information). By comparison, the number of hydrogen bonds per $\{Mo_3\}$ subunit is 1 and 0.5 for **Mo_{12}−Ale−2C** and **Mo_6−Ale−2C**, respectively (i.e., the least-performing photochromic materials of the two series), and their number of potential reducible Mo^{6+} sites is low. For materials with the same number of N−H···O interactions, their positioning toward the POM plays also a key role, because it is well-illustrated by comparing the photochromic properties of the closely related compounds **Mo_6−Ale−1C_a** and **Mo_6−Ale−1C_b**. Both materials are made of the same $[(Mo_3O_8)_2O(O_3PC(C_3H_6NH_2(CH_3))(O)PO_3)_2]^{6-}$ polyanion, but their structures differ by the nature of the associated counter-cations and the number of crystallized water molecules. The different packings induce drastic changes in the hydrogen-bonding networks (Figure 1c). **Mo_6−Ale−1C_a** presents two short intramolecular hydrogen bonds involving the monomeric $\{MoO_6\}$ octahedra ($d_{N\cdots O}$ = 2.790 Å), while **Mo_6−Ale−1C_b** exhibits one short intramolecular hydrogen bond with the $\{MoO_6\}$ monomer ($d_{N\cdots O}$ = 2.802 Å) and one longer intermolecular N−H···O interaction with the $\{Mo_2O_9\}$ dimer ($d_{N\cdots O}$ = 2.894 Å) (see Figure 1c). This drastically impacts their photochromic performances. Indeed, **Mo_6−Ale−1C_b** has a much higher coloration speed, compared to **Mo_6−Ale−1C_a**, with a relative coloration rate constant $k_{Mo_6-Ale-1C_b}/k_{Mo_6-Ale-1Ca}$ of ∼ 5.5, even if **Mo_6−Ale−1C_b** contains longer N−H···O interactions. In first approximation, this should be explained considering that, in the $\{Mo_3\}$ subunit, the photochromism mechanism is more effective when it involves the $\{Mo_2O_9\}$ dimer rather than the $\{MoO_6\}$ monomer (i.e., the $\{Mo_2O_9\}$ dimer should be more easily reducible than the monomeric $\{MoO_6\}$ octahedra). In the same way, **Mo_6−1C−Ale** and **Mo_6−Ale−1C_b** have similar photochromic responses ($k_{Mo_6-1C-Ale}/k_{Mo_6-Ale-1Cb}$ = 0.98, Supporting Information Table SI3), because, similarly as **Mo_6-Ale-1C_b**, **Mo_6-1C-Ale** possesses one intermolecular hydrogen bond involving the same O atom of the $\{Mo_2O_9\}$ dimer with a comparable N···O distance ($d_{N\cdots O}$ = 2.924 Å). Finally, similar reasoning allows an explanation of why **Mo_{12}−Ale−2C** has the slowest coloration speed of the $\{Mo_{12}\}$ series, because it possesses one hydrogen bond per $\{Mo_3\}$ subunit involving only the monomeric $\{MoO_6\}$ octahedron ($d_{N\cdots O}$ = 2.848 Å) (Figure 1a). However, the electrochemistry studies presented here indicate that the sole consideration of Mo^{6+}/Mo^{5+} redox potential is not sufficient for discriminating the reducibility of both the $\{MoO_6\}$ monomer and the $\{Mo_2O_9\}$ dimer, and for explaining the relative kinetics of these two compounds. Second, concerning the nature of the inorganic core, it is observed that, for materials that contain the same grafted bisphosphonate ligand, the coloration speed is faster for $\{Mo_6\}$ species than for $\{Mo_{12}\}$ ones, except for **Mo_6−Ale−1C_b**. However, the electrochemical studies reported here show that the $\{Mo_{12}\}$ and $\{Mo_6\}$ series have quasi-similar redox properties, confirming that a direct correlation between the coloration kinetics and the redox potential of a material is unlikely. Third, among the seven reported materials, **Mo_{12}−Ale** and **Mo_{12}−Ale−1C** have the same $\{Mo_{12}\}$ core and a comparable number of N−H···O interactions (see Figure 1a and Table SI1 in the Supporting Information). This can allow correlating the coloration speed with the nature of the grafted bisphosphonate ligand. In both materials, the N atoms of the ammonium heads preferentially develop quasi-similar intramolecular hydrogen bonds with the $\{Mo_2O_9\}$ dimer (only an additional intermolecular hydrogen bond involving one $\{Mo_3\}$ subunit is observed in **Mo_{12}−Ale**). Consequently, as **Mo_{12}−Ale−1C** shows a coloration speed faster than **Mo_{12}−Ale** (the relative coloration rate constant $k_{Mo_{12}-Ale-1C}/k_{Mo_{12}-Ale}$ is ∼1.7 (see Table SI3 in the Supporting Information), it should be reasonably assumed that the $\{-NH_2Me\}^+$ groups in **Mo_{12}−Ale−1C** have a beneficial effect on the coloration speed of the material. Unfortunately, **Mo_{12}−Ale−2C** cannot be compared to the other members of the $\{Mo_{12}\}$ series, because the hydrogen-bonding network strongly differs in this material, with the $\{-NHMe_2\}^+$ groups developing only intermolecular hydrogen bonds with the monomeric $\{MoO_6\}$ octahedra (see Table SI1 in the Supporting Information). Similarly, such a direct correlation cannot be established in the $\{Mo_6\}$ series. Finally, we can also notice that the great number of crystallized water molecules competing with the O atoms of the POM units for the formation of hydrogen bonds probably accounts for the difficulty to establish unambiguous optical properties/structure correlations.

To summarize, simple spider charts are useful to easily display, at a qualitative level, the performances of the photochromic responses of the seven reported materials and **Mo_{12}−Ale**, as a function of the pertinent parameters discussed above (see Table SI1 and Figure SI8 in the Supporting Information). Because the influence of the degree of methylation of the ammonium group of the functionalized alendronate ligands on the coloration speeds has not been clearly evidenced, this parameter has not been considered as a variable in the diagrams. Nevertheless, we can highlight that **Mo_6−Ale**, which combines a $\{Mo_6\}$ core and a great number of hydrogen bonds involving mainly the alendronate ligand and the $\{Mo_2O_9\}$ dimer, represents a highly efficient photochromic material considering the previously reported photochromic POM systems.

3. CONCLUSION

We have then shown here that it is possible to develop an entire family of intrinsic photochromic polyoxomolybdate materials. The optical properties of such systems can be strongly modulated by playing either on the organic part or the inorganic core constituting these species. While the number of parameters influencing the optical performances of these materials (the number and nature of the intermolecular or intramolecular hydrogen bonds, electrochemical characteristics) makes it difficult to clearly correlate the observed photochromic response of a given material with its topology, this work

dx.doi.org/10.1021/ic202299d | Inorg. Chem. 2012, 51, 2291−2302

highlights that very efficient systems can be obtained using the synthetic strategy developed here, as evidenced in particular by the optical properties of the **Mo_6–Ale** compound. Besides, electrochemical studies have shown that it is possible to easily deposit these compounds on a surface. The characterization and the optical study of films deposited on indium tin oxide (ITO) electrodes will be performed. The covalent connection of photoactive organic molecules via the N atom of the bisphosphonate ligand to such hybrid POMs is also under study.

EXPERIMENTAL SECTION

The complex $Na_2Rb_6[(Mo_3O_8)_4(O_3PC(C_3H_6NH_3)(O)PO_3)_4]\cdot 43H_2O$ (**Mo_{12}–Ale**),[7] the alendronic acid $[H_2O_3PC(C_3H_6NH_2)(OH)PO_3H_2]$ (**Ale**),[17a] the ligand $[H_2O_3PC(C_3H_6NH(CH_3))(OH)PO_3H_2]$ (**Ale–1C**),[17b] the ligand $[H_2O_3PC(C_3H_6N(CH_3)_2)(OH)PO_3H_2]$ (**Ale–2C**),[17c] and the ligand $[H_2O_3PC(C_4H_8NH_2)(OH)PO_3H_2]$ (**1C–Ale**),[17d] have been synthesized as previously reported.

Synthesis of $Na_2Rb_6[(Mo_3O_8)_4(O_3PC(C_3H_6NH_2CH_3)(O)PO_3)_4]\cdot 23H_2O$ (Mo_{12}–Ale–1C). To a solution of $Na_2MoO_4\cdot 2H_2O$ (0.500 g, 2.0 mmol) in 5 mL of water was added **Ale–1C** (0.181 g, 0.69 mmol). 6 M Hydrochloric acid was added dropwise until pH 3.0 was reached. The solution was then stirred for 30 min before the addition of solid RbCl (0.300 g, 2.48 mmol). The solution was allowed to stir for another 1 h, during which time a fine white powder slowly precipitated. This solid was filtered off and the filtrate left to slowly evaporate at room temperature. Colorless crystals were collected the following day. Yield: 0.092 g (15% based on Mo). ^{31}P NMR (200 MHz, D_2O, 25 °C): δ 24.71 and 19.68 (AB spin system, ^2J = 40.6 Hz). ^{1}H NMR (200 MHz, D_2O, 25 °C): δ 3.44–2.95 (m, 2H, CH_2), 2.65 (s, 3H, CH_3), 2.71–2.21 (m, 2H, CH_2), 1.97–1.69 (m, 2H, CH_2). Anal. Calc. for $C_{20}H_{90}Mo_{12}N_4Na_2O_{83}P_8Rb_6$ (found): C 6.54 (6.43), H 2.47 (2.02), N 1.52 (1.45), P 6.75 (6.87), Mo 31.35 (31.07), Na 1.25 (1.58), Rb 13.96 (14.35). IR (KBr pellets): ν (cm^{-1}) = 1645 (m), 1466 (mw), 1458 (mw), 1425 (w), 1356 (vw), 1169 (s), 1125 (sh), 1051 (s), 1025 (s), 927 (sh), 888 (s), 802 (s), 697 (s), 653 (sh), 555 (w).

Synthesis of $Na_4K_4[(Mo_3O_8)_4(O_3PC(C_3H_6NH(CH_3)_2)(O)PO_3)_4]\cdot 38H_2O$ (Mo_{12}–Ale–2C). To a solution of $Na_2MoO_4\cdot 2H_2O$ (0.500 g, 2.0 mmol) in 5 mL of water was added **Ale–2C** (0.191 g, 0.69 mmol). 6 M hydrochloric acid was added dropwise to pH 3.0. The solution was then stirred for 30 min before the addition of solid KCl (0.200 g, 2.68 mmol). The solution was allowed to stir for another 1 h. The white powder was filtered off and the filtrate left to evaporate at room temperature. Colorless crystals were collected the following day. Yield: 0.100 g (16% based on Mo). ^{31}P NMR (200 MHz, D_2O, 25 °C): δ 24.77 and 19.75 (AB spin system, ^2J = 40.1 Hz). ^{1}H NMR (200 MHz, D_2O, 25 °C): δ 3.80–2.54 (m, 2H, CH_2), 2.83 (s, 3H, CH_3), 2.79 (s, 3H, CH_3), 2.71–2.15 (m, 2H, CH_2), 2.03–1.78 (m, 2H, CH_2). Anal. Calc. for $C_{24}H_{128}K_4Mo_{12}N_4Na_4O_{98}P_8$ (found): C 7.81 (7.77), H 3.50 (3.05), N 1.52 (1.48), P 6.71 (6.42), Mo 31.21 (31.16), Na 2.49 (2.67), K 4.24 (4.50). IR (KBr pellets): ν (cm^{-1}) = 1635 (m), 1458 (mw), 1175 (sh), 1122 (sh), 1054 (s), 1028 (sh), 925 (s), 890 (s), 794 (s), 692 (s), 658 (sh), 557 (m), 409 (vw).

Synthesis of $Rb_{0.25}(NH_4)_{5.75}[(Mo_3O_8)_2O(O_3PC(C_3H_6NH_3)(O)PO_3)_2]\cdot 10H_2O$ (Mo_6–Ale). Six hundred sixty milligrams (660 mg) of $(NH_4)_6Mo_7O_{24}\cdot 4H_2O$ (0.53 mmol) are dissolved in 10 mL of water before 328 mg (1.25 mmol, 0.33 eq/Mo) of **Ale** are added. The solution is subjetced to stirring at ambient temperature until all the alendronic acid is dissolved (ca. 5 min). 2 M HCl is then added dropwise until reaching pH = 2.5. The solution is further let stirring for *ca.* one hour before 200 mg of solid RbCl are added. A white powder precipitates. The resulting suspension is stirred for approximately one-half hour at 0 °C before the solid is filtrated and dried with ethanol and diethyl ether (yield: 707 mg). The totality of this powder is dissolved in 50 mL of 2 M NH_4OAc/AcOH buffer. The few insoluble impurities are removed by centrifugation, and the solution is left to evaporate slowly at room temperature, affording big needle-shaped crystals, stable to air, after 5 days. Yield: 447 mg (40% based on Mo). ^{31}P NMR (200 MHz, D_2O, 25 °C): δ 21.63 (s, 1.8 P), 21.36 (s, 0.2 P). ^{1}H NMR (200 MHz, D_2O, 25 °C): δ 3.00 (t, 2H, CH_2, ^3J = 6.7 Hz), 2.16–1.84 (m, 4H, CH_2). Anal. Calc. for $Mo_6P_4C_8H_{61.25}N_{7.75}O_{41}Rb_{0.25}$ (found): C 5.85 (6.15), H 3.76 (3.78), N 6.61 (6.81), P 7.54 (7.53), Mo 35.03 (34.43), Rb 1.33 (1.75). IR (KBr pellets): ν (cm^{-1}) = 1505 (m), 1416 (s), 1149 (s), 1125 (sh), 1075 (s), 1034 (m,sh), 1022 (m), 981 (w), 910 (vs), 884 (s), 867 (s), 823 (w), 734 (m), 693 (m), 638 (m).

Synthesis of $Rb_{0.25}(NH_4)_{5.75}[(Mo_3O_8)_2O(O_3PC(C_3H_6NH_2(CH_3))(O)PO_3)_2]\cdot 12H_2O$ (Mo_6–Ale–1C$_a$). To a solution of $(NH_4)_6Mo_7O_{24}\cdot 4H_2O$ (0.660 g, 0.53 mmol) in 10 mL of water was added **Ale–1C** (0.329 g, 1.25 mmol). The solution is allowed to stir for 10 min. A 2 M hydrochloric acid was added dropwise to pH 2.5. The solution was then stirred for 1 h before the addition of solid RbCl (0.600 g, 4.96 mmol). The solution was subjected to stirring for another 2 h. The white powder is filtrated and dried with ethanol and diethyl ether (yield: 0.940 g). The totality of this solid is dissolved in 70 mL of 1 M CH_3COONH_4/CH_3COOH buffer. The insoluble impurities are removed by centrifugation and the solution is left to evaporate at room temperature. Needle-shaped crystals were collected after five days. Yield: 0.510 g (48% based on Mo). ^{31}P NMR (200 MHz, D_2O, 25 °C): δ 21.55 (s, 1.8 P), 21.39 (s, 0.2 P). ^{1}H NMR (200 MHz, D_2O, 25 °C): δ 2.99 (t, 2H, CH_2, ^3J = 7.8 Hz), 2.78 (s, 2.7H, CH_3), 2.69 (s, 0.3H, CH_3), 2.13–1.84 (m, 4H, CH_2CH_2). Anal. Calc. for $C_{10}H_{69}Mo_6N_{7.75}O_{43}P_4Rb_{0.25}$ (found): C 7.03 (7.28), H 4.07 (3.65), N 6.36 (6.23), P 7.26 (6.94), Mo 33.72 (32.47), Rb 1.25 (1.37). IR (KBr pellets): ν (cm^{-1}) = 1624 (m), 1403 (sh), 1158 (s), 1135 (s), 1076 (s), 1035 (w), 1008 (w), 911 (s), 879 (s), 809 (vw), 683 (sh), 632 (sh), 555 (w), 525 (w), 484 (vw).

Synthesis of $Cs_{1.25}K_{0.25}(NH_4)_{4.5}[(Mo_3O_8)_2O(O_3PC(C_3H_6NH_2(CH_3))(O)PO_3)_2]\cdot 9H_2O$ (Mo_6–Ale–1C$_b$). To a solution of $(NH_4)_6Mo_7O_{24}\cdot 4H_2O$ (0.660 g, 0.53 mmol) in 10 mL of water was added **Ale–1C** (0.329 g, 1.25 mmol). The solution is subjected to stirring for 10 min. 2 M hydrochloric acid was added dropwise to pH 2.5. The solution was then stirred for 1 h before the addition of solid KCl (0.500 g, 6.71 mmol) and solid CsCl (0.300 g, 2.26 mmol). The solution was allowed to stir for another 1 h. The white powder is filtrated and dried with ethanol and diethyl ether (yield: 0.725 g). The totality of this solid is dissolved in 50 mL of 1 M CH_3COONH_4/CH_3COOH buffer. The insoluble impurities are removed by centrifugation and the solution is left to evaporate at room temperature. Colorless crystals were collected after five days. Yield: 0.400 g (42% based on Mo). ^{31}P NMR (200 MHz, D_2O, 25 °C): δ 21.53 (s). ^{1}H NMR (200 MHz, D_2O, 25 °C): δ 2.99 (t, 2H, CH_2, ^{3}J = 6.7 Hz), 2.78 (s, 2.4H, CH_3) and 2.69 (s, 0.6H, CH_3), 2.22–1.74 (m, 4H, CH_2). Anal. Calc. for $C_{10}H_{58}Mo_6N_{6.5}O_{40}P_4Cs_{1.25}K_{0.25}$ (found): C 6.73 (6.70), H 3.27 (3.32), N 5.10 (5.26), P 6.94 (6.86), Mo 32.25 (32.12), Cs 9.31 (9.57), K 0.55 (0.16). IR (FTR): ν (cm^{-1}) = 1624 (w), 1403 (s), 1160 (s), 1134 (s), 1076 (s), 1035 (m), 1008 (m), 911 (vs), 979 (vs), 809 (w), 683 (sh), 632 (sh), 555 (m), 548 (m), 612 (sh), 484 (w).

Synthesis of $(NH_4)_4K_2[(Mo_3O_8)_2O(O_3PC(C_3H_6NH(CH_3)_2)(O)PO_3)_2]\cdot 7H_2O$ (Mo_6–Ale–2C). $(NH_4)_6Mo_7O_{24}\cdot 4H_2O$ (0.330 g, 0.265 mmol), **Ale–2C** (0.172 g, 0.625 mmol) and potassium chloride (0.300 g, 4.02 mmol) in 8 mL of 0.5 M CH_3COONH_4/CH_3COOH. This mixture was sealed in a 23-mL Teflon-lined stainless steel reactor before heating to 130 °C over a period of 4 h, kept at this temperature for 20 h, and cooled to room temperature over a period of 36 h. The resulting mixture was filtered and the filtrate left to evaporate at room temperature. Needle-shaped crystals were collected after four days. Yield: 0.290 g (56% based on Mo). ^{31}P NMR (200 MHz, D_2O, 25 °C): δ 21.33 (s, 0.5 P), 21.19 (s, 1.5 P). ^{1}H NMR (200 MHz, D_2O, 25 °C): δ 3.19–3.08 (m, 2H, CH_2), 2.96 (s, 2H, CH_3), 2.85 (s, 4H, CH_3), 2.18–1.82 (m, 4H, CH_2). Anal. Calc. for $C_{12}H_{56}K_2Mo_6N_6O_{38}P_4$ (found): C 8.63 (8.75), H 3.38 (3.41), N 5.03 (5.21), P 7.42 (7.10), Mo 34.46 (34.95), K 4.68 (5.08). IR (KBr pellets): ν (cm^{-1}) = 1617 (m), 1462 (m), 1436 (m), 1161 (s), 1137 (s), 1073 (s), 1034 (m), 1013 (m), 916 (vs), 885 (s), 866 (s), 831 (vw), 743 (s), 687 (s), 647 (s).

Synthesis of $(NH_4)_6[(Mo_3O_8)_2O(O_3PC(C_4H_8NH_3)(O)PO_3)_2]\cdot 10H_2O$ (Mo_6–1C–Ale). $(NH_4)_6Mo_7O_{24}\cdot 4H_2O$ (0.330 g, 0.265 mmol) and **1C–Ale** (0.164 g, 0.625 mmol) in 8 mL of 0.5 M

dx.doi.org/10.1021/ic202299d | *Inorg. Chem.* 2012, 51, 2291–2302

CH_3COONH_4/CH_3COOH was sealed in a 23 mL Teflon-lined stainless steel reactor before heating to 130 °C over a period of 4 h, kept at this temperature for 20 h, and cooled to room temperature over a period of 36 h. The resulting mixture was filtered and the filtrate left to evaporate at room temperature. Needle-shaped crystals were collected after five days. Yield 0.230 g (45% based on Mo). ^{31}P NMR (200 MHz, D_2O, 25 °C): δ 22.23 (s, 0.2 P), 21.19 (s, 1.8 P). ^1H NMR (200 MHz, D_2O, 25 °C): δ 3.22 and 3.02 (2 br, 2H, CH_2), 1.98−1.69 (m, 6H, CH_2). Anal. Calc. for $C_{10}H_{66}Mo_6N_8O_{41}P_4$ (found): C 7.26 (7.29), H 4.02 (4.02), N 6.77 (6.85), P 7.49 (7.25), Mo 34.80 (35.01). IR (KBr pellets): ν (cm^{-1}) = 1650 (m), 1623 (m), 1502 (m), 1401 (sh), 1148 (s), 1120 (s), 1079 (s), 1043 (s), 988 (m), 923 (vs), 885 (s), 830 (vw), 739 (m), 718 (m), 649 (w), 527 (w).

X-ray Crystallography. Data collections were carried out at room temperature for all the structures, using a Siemens SMART three-circle diffractometer equipped with a CCD bidimensional detector with the monochromatized wavelength λ(Mo Kα) = 0.71073 Å, except for compound **Mo_6-Ale-1C_b** for which data collection was carried out on a Brüker Nonius X8 APEX 2 diffractometer. Absorption corrections were based on multiple and symmetry-equivalent reflections in the dataset using the SADABS program,[18] based on the method of Blessing.[19] Structures were solved by direct methods, and refined by full-matrix least-squares using the SHELX-TL package.[20] In all the structures, there is a discrepancy between the formulas determined by elemental analysis and that deduced from the crystallographic atom list, because of the difficulty in locating all the disordered water molecules and alkali counterions. Disordered water molecules and alkali counterions were thus refined with partial occupancy factors. In the structure of **Mo_6−Ale**, **Mo_6−Ale−1C_a**, **Mo_6−Ale−1C_b**, **Mo_6−Ale−2C** and **Mo_6−1C−Ale**, NH_4^+, and H_2O could not be distinguished based on the observed electron densities; therefore, all positions were labeled as O and assigned the oxygen atomic diffusion factor. The H atoms were theoretically located on the basis of the conformation of the supporting atoms. Crystallographic data are given in Table 1.

CCDC −864375 (**Mo_{12}−Ale−1C**), −864376 (**Mo_{12}−Ale−2C**), −864377 (**Mo_6−Ale**), −864378 (**Mo_6−Ale−1C_a**), −864379 (**Mo_6−Ale−1C_b**), −864380 (**Mo_6−Ale−2C**), and −864381 (**Mo_6−1C−Ale**) contain the supplementary crystallographic data, which can be obtained free of charge from the Cambridge Crystallographic Data Centre via www.ccdc.cam.ac.uk/data_request/cif.

NMR Measurements. ^{31}P NMR spectra were recorded with ^1H decoupling on a Brüker AC-200 spectrometer operating at 81 MHz for room temperature experiments and on a Brüker AC-300 spectrometer operating at 121.5 MHz for the 275−350 K experiments performed on compound **Mo_6−Ale−1C_a**, using 5-mm tubes. ^{31}P chemical shifts were referenced to the external standard of 85% H_3PO_4. For all compounds, ∼20 mg of sample were dissolved in 700 μL of D_2O. The concentrations thus varied between 2 mM and 8 mM. ^1H NMR spectra were recorded on a Brüker AC-200 spectrometer operating at 200 MHz, using 5 mm tubes.

Infrared Spectra. Infrared (IR) spectra were recorded on an IRFT Magna 550 Nicolet spectrophotometer, using KBr pellets.

Scanning Electron Microscopy. Scanning electron microscopy (SEM) observations were performed with a JEOL Model JSM-5800 LV apparatus.

Electrochemical Studies. Pure water was used throughout. It was obtained by passing water through a RiOs 8 unit, followed by a Millipore-Q Academic purification set. All reagents were of high-purity grade and were used as purchased without further purification. The electrolyte was a 0.5 M Li_2SO_4 aqueous solution with the pH adjusted to 3.0 via the addition of H_2SO_4. The solutions were deaerated thoroughly for at least 30 min, with pure argon, and kept under a positive pressure of argon during the experiments. The source, mounting and polishing of the glassy carbon (GC, Carbone Lorraine, France) electrodes have been described.[21] The glassy carbon samples had a diameter of 3 mm. The auxiliary electrode was a platinum plate placed within a fritted-glass isolation chamber. Potentials are quoted against a saturated calomel electrode (SCE). The electrochemical setup was an EG&G 273 A driven by a PC with the M270 software. All experiments were performed at room temperature.

Diffuse Reflectance Spectroscopy. Diffuse reflectivity spectra were collected at room temperature on a finely ground sample with a Cary 5G spectrometer (Varian) equipped with a 60 mm diameter integrating sphere and computer control using the "Scan" software. Diffuse reflectivity was measured from 250 to 1550 nm (i.e., from 5 to 0.8 eV) with a 2 nm step using Halon powder (from Varian) as reference (100% reflectance). The samples were irradiated with a Fisher Bioblock labosi UV lamp (λ_{exc} = 365 nm or 254 nm, P = 12W).

■ ASSOCIATED CONTENT

Ⓢ Supporting Information

This material is available free of charge via the Internet at http://pubs.acs.org.

■ AUTHOR INFORMATION

Corresponding Author

*Fax: (+33)240-373-995 (R.D.), (+33)139-254-381 (P.M.). E-mail: remi.dessapt@cnrs-imn.fr (R.D.), mialane@chimie.uvsq.fr (P.M.).

■ ACKNOWLEDGMENTS

E. Cadot is gratefully acknowledged for fruitful discussions on the NMR behavior of the {Mo_6} compounds. This work was supported by the CNRS, the Ministère de l'Enseignement Supérieur et de la Recherche and the ANR-11-BS07-011-01 BIOOPOM.

■ REFERENCES

(1) Pope, M. T. *Heteropoly and Isopoly Oxometalates*; Springer−Verlag: New York, 1983.

(2) (a) Song, Y.-F.; Long, D.-L.; Ritchie, C.; Cronin, L. *Chem. Record* **2011**, *11*, 158. (b) Dolbecq, A.; Dumas, E.; Mayer, C.; Mialane, P. *Chem. Rev.* **2010**, *110*, 6009. (c) Gouzerh, P.; Proust, A. *Chem. Rev.* **1998**, *98*, 77.

(3) (a) Song, Y.-F.; McMillan, N.; Long, D.-L.; Kane, S.; Malm, J.; Rielhe, O. M.; Pradeep, C. P.; Gadegaard, N.; Cronin, L. *J. Am. Chem. Soc.* **2009**, *131*, 1340. (b) Lu, M.; M. Nolte, W.; He, T.; Cortley, D. A.; Tour, J. M. *Chem. Mater.* **2009**, *27*, 442.

(4) (a) Lu, M.; Xie, B.; Kang, J.; Chen, F.-C.; Yang, Y.; Peng, Z. *Chem. Mater.* **2005**, *17*, 402. (b) Kang, J.; Xu, B.; Peng, Z.; Zhu, X.; Wei, Y.; Powell, D. R. *Angew. Chem., Int. Ed.* **2005**, *44*, 6902.

(5) (a) Han, J. W.; Hill, C. L. *J. Am. Chem. Soc.* **2007**, *129*, 15094. (b) Wang, X.-L.; Li, Y.-G.; Lu, Y.; Fu, H.; Su, Z.-M.; Wang, E.-B. *Cryst. Growth Des.* **2010**, *10*, 2227. (c) Albelo, L. M. R.; Ruiz-Salvador, A. R.; Sampieri, A.; Lewis, D. W.; Gómez, A.; Nohra, B.; Mialane, P.; Marrot, J.; Sécheresse, F.; Mellot-Draznieks, C.; Ngo Biboum, R.; Keita, B.; Nadjo, L.; Dolbecq, A. *J. Am. Chem. Soc.* **2009**, *131*, 16078. (d) Nohra, B.; El Moll, H.; Rodriguez Albelo, L. M.; Mialane, P.; Marrot, J.; Mellot-Draznieks, C.; O'Keeffe, M.; Ngo Biboum, R.; Lemaire, J.; Keita, B.; Nadjo, L.; Dolbecq, A. *J. Am. Chem. Soc.* **2011**, *133*, 13363.

(6) (a) Bar Nahum, I.; Neumann, R. *Chem. Commun.* **2003**, 2690. (b) Bonchio, M.; Carraro, M.; Scorrano, G.; Bagno, A. *Adv. Synth. Catal.* **2004**, *346*, 648.

(7) Compain, J.-D.; Mialane, P.; Marrot, J.; Sécheresse, F.; Zhu, W.; Oldfield, E.; Dolbecq, A. *Chem.—Eur. J.* **2010**, *16*, 13441.

(8) (a) He, T.; Yao, J. *Prog. Mater. Sci.* **2006**, *51*, 810. (b) Hubbard, D. J.; Johnston, A. R.; Sanchez Casalongue, H.; Narducci Sarjeant, A. N.; Norquist, A. J. *Inorg. Chem.* **2008**, *47*, 8518.

(9) (a) Zhang, X.-M.; Shan, B.-Z.; Duan, C.-Y.; You, X.-Z. *Chem. Commun.* **1997**, 1131. (b) Compain, J.-D.; Mialane, P.; Dolbecq, A.; Marrot, J.; Proust, A.; Nakatani, K.; Yu, P.; Sécheresse, F. *Inorg. Chem.* **2009**, *48*, 6222.

(10) (a) Yamase, T. *Chem. Rev.* **1998**, *98*, 307. (b) Dessapt, R.; Collet, M.; Coué, V.; Bujoli-Doeuff, M.; Jobic, S.; Lee, C.; Whangbo,

M.-H. *Inorg. Chem.* **2009**, *48*, 574. (c) Dessapt, R.; Gabard, M.; Bujoli-Doeuff, M.; Deniard, P.; Jobic, S. *Inorg. Chem.* **2011**, *50*, 8790.
(11) Pardo, R.; Zayat, M.; Levy, D. *Chem. Soc. Rev.* **2011**, *40*, 672.
(12) (a) Kortz, U.; Pope, M. T. *Inorg. Chem.* **1995**, *34*, 3848. (b) Kortz, U.; Pope, M. T. *Inorg. Chem.* **1995**, *34*, 2160. (c) Tan, H.; Chen, W.; Liu, D.; Li, Y.; Wang, E. *Dalton Trans.* **2004**, 1259. (d) du Peloux, C.; Dolbecq, A.; Mialane, P.; Marrot, J.; Sécheresse, F. *Dalton Trans.* **2004**, 1259. (e) Dolbecq, A.; Lisnard, L.; Mialane, P.; Marrot, J.; Bénard, M.; Rohmer, M.-M.; Sécheresse, F. *Inorg. Chem.* **2006**, *45*, 5898. (f) Dolbecq, A.; Compain, J.-D.; Mialane, P.; Marrot, J.; Sécheresse, F.; Keita, B.; Brudna Hozle, L. R.; Miserque, F.; Nadjo, L. *Chem.—Eur. J.* **2009**, *15*, 733. (g) Banerjee, A.; Bassil, B. S.; Röschenthaler, G.-V.; Kortz, U. *Eur. J. Inorg. Chem.* **2010**, 3915. (h) Banerjee, A.; Raad, F. S.; Vankova, N.; Bassil, B. S.; Heine, T.; Kortz, U. *Inorg. Chem.* **2011**, *50*, 11667.
(13) Compain, J.-D.; Deniard, P.; Dessapt, R.; Dolbecq, A.; Oms, O.; Sécheresse, F.; Marrot, J.; Mialane, P. *Chem. Commun.* **2010**, *46*, 7733.
(14) Sergienko, V. S. *Crystallogr. Rep.* **1999**, *44*, 877.
(15) Tan, H.; Chen, W.; Liu, D.; Feng, X.; Li, Y.; Yan, A.; Wang, E. *Dalton Trans.* **2011**, *40*, 8414.
(16) Coué, V.; Dessapt, R.; Bujoli-Doeuff, M.; Evain, M.; Jobic, S. *Inorg. Chem.* **2007**, *46*, 2824.
(17) (a) Kubíček, V.; Kotek, J.; Hermann, P.; Lukeš, I. *Eur. J. Inorg. Chem.* **2007**, 333. (b) Lolli, M. L.; Rolando, B.; Tosco, P.; Chaurasia, S.; Di Stilo, A.; Lazzarato, L.; Gorassini, E.; Ferracini, R.; Oliaro-Bosso, S.; Fruttero, R.; Gasco, A. *Bioorg. Med. Chem.* **2010**, *18*, 2428. (c) Klenner, T.; Wingen, F.; Keppler, B. K.; Krempien, B.; Schmähl, D. *J. Cancer. Res. Clin. Oncol.* **1990**, *116*, 341. (d) Kieczykowski, G. R.; Jobson, R. B.; Melillo, D. G.; Reinhold, D. F.; Grenda, V. J.; Shinkai, I. *J. Org. Chem.* **1995**, *60*, 8310.
(18) Sheldrick, G. M. *SADABS, Program for Scaling and Correction of Area Detector Data*; University of Göttingen: Göttingen, Germany, 1997.
(19) Blessing, R. *Acta Crystallogr., Sect. A: Found. Crystallogr.* **1995**, *A51*, 33.
(20) Sheldrick, G. M. *SHELX-TL, version 5.03, Software Package for the Crystal Structure Determination*; Siemens Analytical X-ray Instrument Division: Madison, WI, 1994.
(21) Keita, B.; Nadjo, L. *J. Electroanal. Chem.* **1988**, *243*, 87103.